THE JOURNAL OF PHYSICAL CHEMISTRY C

ARTICLE

pubs.acs.org/JPCC

Programmable Surface Architectures Derived from Hybrid Polyoxometalate-Based Clusters

Chiara Musumeci,[†] Alessandro Luzio,[‡] Chullikkattil P. Pradeep,[§] Haralampos N. Miras,[§] Mali H. Rosnes,[§] Yu-Fei Song,[§] De-Liang Long,[§] Leroy Cronin,*[,§] and Bruno Pignataro*[,∥]

[†]Superlab-Consorzio Catania Ricerche, Stradale Primosole 50, 95121, Catania, Italy

[‡]Dipartimento di Ingegneria Industriale, Università di Palermo, V.le delle Scienze -90128 Palermo, Italy

[§]Department of Chemistry, WestCHEM, University of Glasgow, Glasgow, G12 8QQ, United Kingdom

[∥]Dipartimento di Chimica "S. Cannizzaro", Università di Palermo, V.le delle Scienze -90128 Palermo, Italy

Supporting Information

ABSTRACT: The exploration of the self-organization of a range of the polyoxometalate-based molecular structures reveals a diverse range of surface patterns and morphologies on solid substrates of technological interest, including methylated and hydroxylated silicon surfaces (namely, $SiCH_3$ and SiOH). By exploiting the interplay between the intrinsic molecular properties and the surface chemistry as well as dynamic spatiotemporal phenomena (e.g., dewetting), we show that these systems can yield 0D, 2D, and 3D architectures via solution deposition at the solid surface, including nanodots, discs, lamellas, porous networks, and layer-by-layer assemblies. In general, we observed that layer-by-layer growth is a common feature on low surface energy $SiCH_3$. In addition, the polyoxometalate derived architectures are able to effectively modulate the drop spreading dynamics on high surface energy SiOH, so that dewetting induces the formation of nanodots from dilute solutions of the precursor POM hybrid, whereas using high concentration results in the formation of complex architectures whose shape depends on the molecular structure of the POM-based building block utilized. Finally, we show that hybrid POM derivatives with one or more functional moieties can be organized in an ordered fashion, thus yielding interesting model systems for the assembly of POM-based multifunctional nanostructures on surfaces.

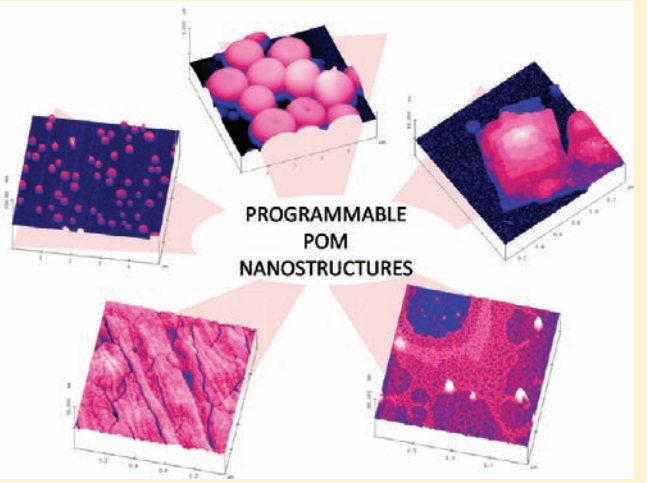

1. INTRODUCTION

The great current interest in polyoxometalates (POMs) reflects the diverse nature of this family of inorganic clusters (which can also be described as molecular metal oxides),[1] which exhibit a wide variety of compositions and structural versatility,[2,3] as well as important optical,[4] catalytic,[5−9] and magnetic[10−13] properties. One important achievement towards the development of a new class of functional materials has been the fabrication of functional films and nanoscale devices on surfaces,[14,15] and the effort to understand the self-organization of POMs on various surfaces as a function of structural features. POM-based monolayers on surfaces like Ag,[16] Au,[17] HOPG,[18,19] etc., as well as multilayers generated by Langmuir−Blodgett techniques[20−22] and electrostatic layer-by-layer assembly[23−25] have been studied over the last two decades for their possible applications in a variety of fields such as catalysis, sensor applications, and nanotechnology. Also, the covalent anchoring of POMs onto gold surfaces[26] using thiol-based derivatized long chains as anchoring groups has also been achieved with good spatial control. However, the majority of these studies are based on common POM structural archetypes such as Keggin, Dawson, Preyssler, etc., clusters and their lacunary and/or cation exchanged derivatives.[27] Although these fundamental studies have laid the basic foundations, the development of true functional POM devices with well-defined architectures could benefit from a comprehensive approach that compares pure clusters, hybrids, and organic-cation encapsulated systems. This information is important since, structural manipulation, via covalent functionalization, has been shown to affect the self-assembly behavior of POMs in solid state and in solution,[28,29] as well as allow the introduction of new functionalities to POMs grafted onto surfaces.[30]

To work towards achieving our goal of fabricating POM-based functional devices, we are interested in understanding the surface

Received: October 15, 2010
Revised: January 10, 2011
Published: February 25, 2011

ACS Publications © 2011 American Chemical Society

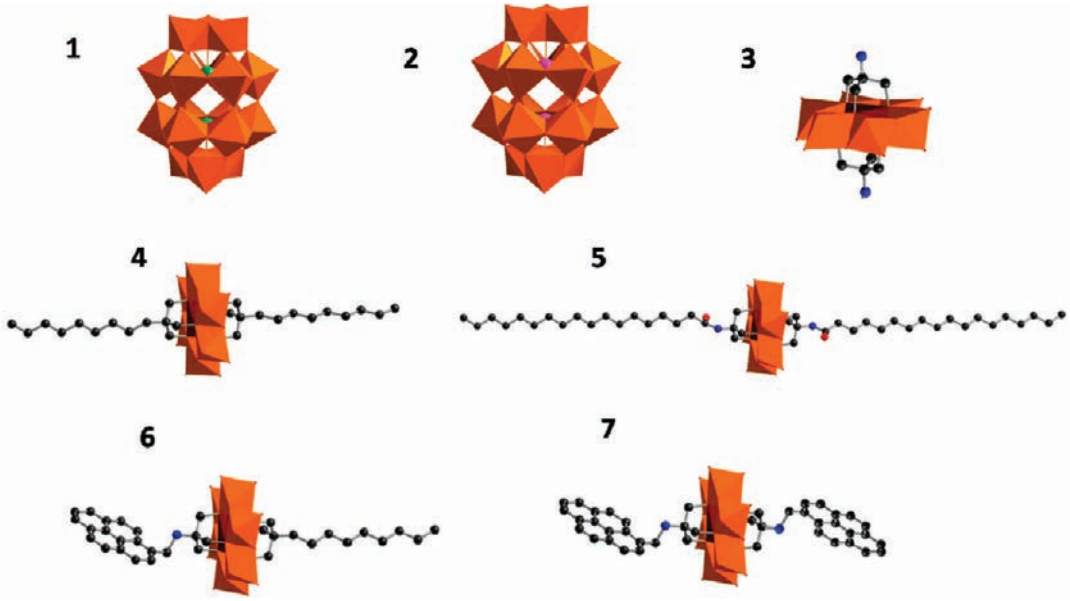

Figure 1. Combined polyhedral and ball-and-stick representations of the cluster anions studied here. Color code: Mo, orange polyhedron; Mn, brown polyhedron; V, green polyhedron; S, pink sphere; C, gray sphere; N, blue sphere; O, red sphere. The H atoms are omitted for clarity.

assembly of new functional clusters and hybrid/multifunctional POMs on substrates of technological interest by employing solution deposition and by exploiting both self-assembly and dynamic self-assembly processes.[31−33] Additionally, the clusters used in this study represents a range of structures, and interesting functionalities such as internal switchability,[34,35] solvent dependent self-assembly,[28] surfactant like properties,[36] etc. These include (Figure 1) a Dawson-type cluster, $TBA_6[H_2VMo_{17}O_{54}(VO_4)_2]$ (**1**), where TBA = $N(C_4H_9)_4$;[37] Dawson-like cluster, $(C_{20}H_{44}N)_4[Mo_{18}O_{60}S_2]$ (**2**) that incorporates two sulfite heteroanions;[34,35] Tris-grafted Mn-Anderson cluster $TBA_3[MnMo_6O_{18}\{(OCH_2)_3C-NH_2\}_2]$ (**3**),[38] where Tris = Tris(hydroxymethyl)aminomethane; Mn-Anderson-based organic−inorganic hybrid cluster $TBA_3[MnMo_6O_{18}\{(OCH_2)_3C-C_9H_{17}\}_2]$ with two grafted C_9 alkene chains (**4**);[39] Mn-Anderson-based organic−inorganic hybrid cluster $TBA_3[MnMo_6O_{18}\{(OCH_2)_3C-NHCO-C_{17}H_{35}\}_2]\cdot 2C_3H_7NO$, having two long C_{18} alkyl chains grafted to either end of a Mn-Anderson cluster via Tris (**5**);[36] Mn-Anderson-based hybrid cluster $TBA_3[MnMo_6O_{18}((OCH_2)_3C-C_9H_{17})-((OCH_2)_3CNH-CH_2-C_{16}H_9)]$ with a C_9 alkene chain on one side and a pyrene group on the other (**6**);[39] and Mn-Anderson-based hybrid cluster $TBA_3[MnMo_6O_{18}\{(OCH_2)_3CNH-CH_2-C_{16}H_9\}_2]$ with two grafted pyrene groups (**7**).[40]

Note that the physical structure of the clusters found in compounds **1**−**3** differs, and we anticipated that the structural features of these clusters would be a crucial driving force for their surface assembly behavior, as also demonstrated by observing surface architectures very similar to those of **1** in several other Dawson-type systems of different structures (see compounds **8**−**13** in Figure S1 of the Supporting Information). In particular, cluster **1** presents the peanut-like shape distinctive of the $\{M_{18}O_{54}\}$ Dawson-type framework; in the Dawson-type cluster **2**, the incorporation of nontetrahedral sulfite ions causes the formation of an atypical Dawson-like[41] cage shape; the Anderson structure of cluster **3** consists of six edge-sharing M_6 octahedra around a central heteroatom forming a planar discoid cage shape. Further, the series **4**−**7** use the same Anderson cluster with the appended Tris (or Tris-like) ligand anchors found in compound **3**. Finally, compounds **6** and **7** with one or two aromatic moieties are reported to address the structural control and the incorporation of active functionalities of potential interest for optical and electronics applications simultaneously.

Herein, we show that it is possible to induce the formation of architectures with a wide variety of shapes and dimensionalities on silicon-based surfaces as a function of the structure of the cluster; nature of the derivatization; solution concentration; film thermal treatments; and nature of the surface, i.e., native silicon oxide modified to yield a high Si−CH_3 or Si−OH surface density.

2. RESULTS AND DISCUSSION

2.1. Layer-by-Layer Assembly of POM-Based Systems on $SiCH_3$. Drop-casting by acetonitrile-based solution on $SiCH_3$ gives rise to irregular architectures whereby good control of the thickness and uniformity of the POM film is not achieved. This is likely due to the dynamics of the deposition governed by the low wettability (the water contact angle on $SiCH_3$ is about 90°), producing remarkable concentration gradients and thermal fluctuations into the fluid during the drop evaporation.[42] As a consequence, large scale images result in structural inhomogeneity (see Figure S2 of the Supporting Information), where the main growth features of compounds **1**−**7** on $SiCH_3$ can be characterized by analyzing the thinnest regions at the substrate surface (see Figure 2).

Independent of their chemical structures, all the studied POM systems show a layer-by-layer (LbL) growth mode, with the related structures being generally associated with a 3D terraced-assembly mode.[43] Section analysis emphasizes the presence of both monolayer and multilayer steps whereby the step height of the terraces is not greatly affected by the thickness of the film. In particular, the growth mode of **1**−**5** appears to be the result of a physical effect governed by "step bunching" defects.[44,45] These phenomena are generally associated with an inefficiency in the molecular step down process characteristic of a LbL growth mode. In particular, due to the presence of an Ehrlich−Schwoebel step-edge barrier, the ascendant molecular flow prevails on

dx.doi.org/10.1021/jp109916e |J. Phys. Chem. C 2011, 115, 4446–4455

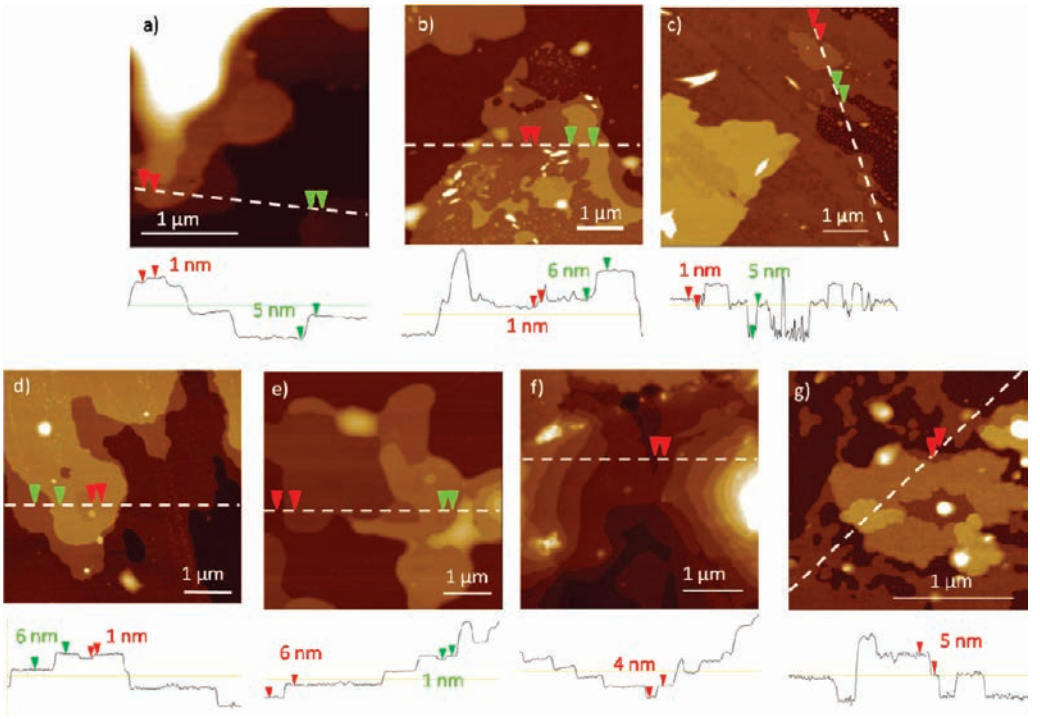

Figure 2. SFM images and section analyses along the dashed lines of compounds **1**−**7** (a−g, respectively) drop-cast on $SiCH_3$.

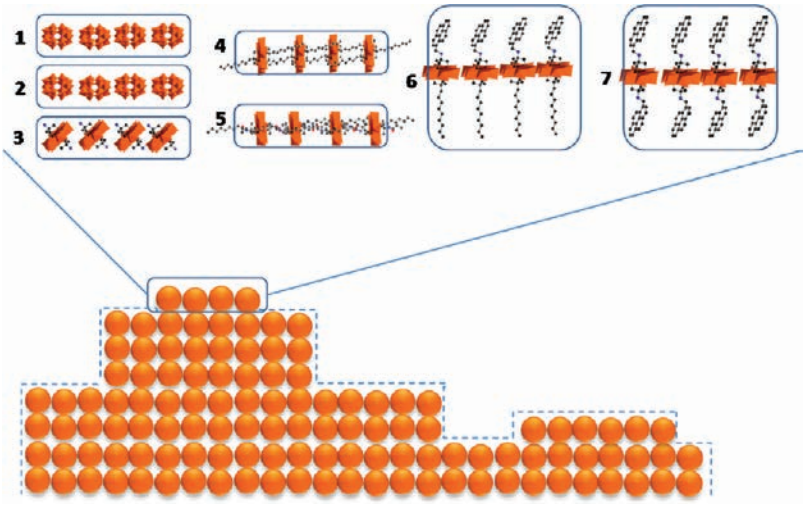

Figure 3. Pictorial sketch showing the LbL organization of POM-based compounds on $SiCH_3$. In the inset, the proposed molecular orientations within the terraces are reported.

the descendent one, allowing for a significant molecular nucleation over the terraces as evidenced by the features seen in Figure 2.[43] Figure 3 gives suggested molecular orientations for the different systems investigated based on the comparison of the observed SFM step heights and the molecular dimensions of the POM clusters. In the case of compounds **6** and **7**, the 4−5 nm tall steps are consistent with monomolecular layers with the long molecular axis perpendicular with respect to the substrate surface.

Such a picture allows us to state that, when a low energy surface is employed, a layer-by-layer architecture is obtained for all the POM compounds studied, with their intermolecular interactions playing a major role with respect to the substrate surface forces.

2.2. Dynamic Surface Assembly of POMs on SiOH. While low energy $SiCH_3$ seems to act as an inert support for the assembly of compounds **1**−**7**, high energy SiOH should have more influence in tuning the structural organization of these systems. Indeed, when POM solutions are dispensed onto SiOH, high spreading occurs, the water contact angle of this surface being typically less than 10°. In contrast to $SiCH_3$, a wide structural homogeneity has typically been observed in the whole drop area. Using SFM, we checked the nanoscale morphology of different points of the drop within an area of tens of mm^2 spanning from the inner parts to the periphery. Only at the very peripheral zone of the drop can different arrangements be observed due to the occurrence of well-known[46,47] chemical gradients and

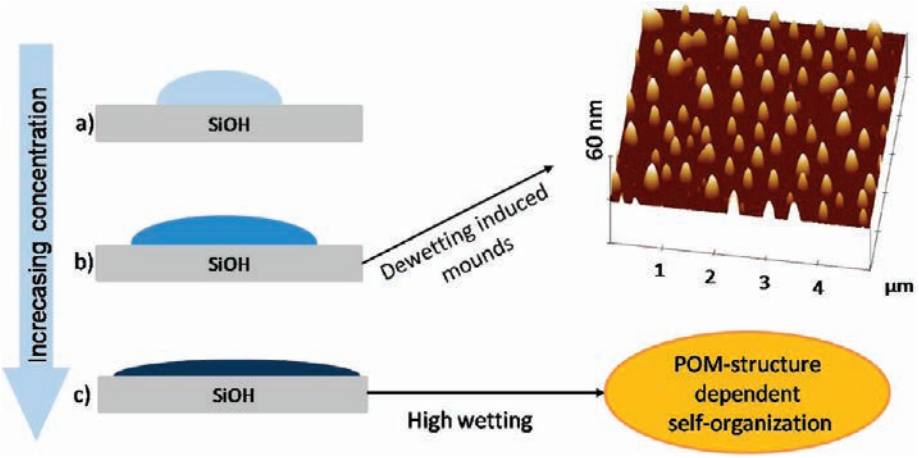

Figure 4. Scheme of the concentration effect on the drop spreading along with the resulting structures: (a) pure acetonitrile solvent; (b) 0.1 mg/mL POM solution in acetonitrile gives dewetted nanodots (the related SFM image for **1** is exemplarily shown, where 5−15 nm tall and 100−300 nm wide nanodots are observed with a density of about 4 dots/μm^2); (c) 1 mg/mL POM solution in acetonitrile resulting in large spreading along with POM-dependent self-structuring.

fluxes at the periphery of the evaporating drop (see as an example Figure S3 of the Supporting Information).

It is interesting to note that the drop spreading at the solid surface interface has been observed to be strongly dependent on the POM concentration. In Figure 4, the dependence of POM concentration on the drop spreading is qualitatively presented. In particular, a significant change of the drop contact area and evaporation time is observed by drop-casting POM solutions with increased concentration from 0 mg/mL (pure solvent) to 1 mg/mL. For example, cluster **1** gives contact diameters of 7 and 11 mm along with evaporation times of 10 and 7 s, respectively, for 1 μL drop solutions of 0.1 and 1 mg/mL, while a 1 μL drop of pure acetonitrile spreads with a contact diameter of 3.5 mm evaporating in 15 s. The above behavior resembles that dealing with the spreading of nanofluids such as dispersion of nanoparticles on a solid surface. It has been observed that the presence of nanoparticles promotes the spreading of a drop on a high energy surface and this was ascribed to the formation of a 2D solid-like region at the three-phase contact line, that produces the advancing of the contact line and a stepwise thinning of the film.[48]

Furthermore, dilute solutions (0.1 mg/mL) of all the POM-based systems here investigated aggregate to yield 0D nanodots (see Figure 4b for **1** and Figure S4 of the Supporting Information for the other POM systems). This common feature can be explained by film instability during the evaporation resulting in a dewetting process. Indeed, during dewetting, the rupture of the liquid film induces hole formation at first and then the growing holes evolve into a network of liquid rims that finally break into droplets.[49]

Thus, simply by varying the POM concentration in the 0.1−1 mg/mL range, we were able to change the dynamic behavior switching from an unstable condition of thicker solution films (dewetting-induced nanodots) to a high wetting and large spreading condition that induces self-organized architectures very sensitive to the peculiar POM structure, whose formation can be explained in terms of structural forces promoted by the formation of ordered thin layers and giving stability to the system.[50] This is also supported by the large spreading observed at increased POM concentrations.[51]

In this respect, it can be anticipated that POMs show the ability to finely tune the spreading of fluids on hydrophilic surfaces along with the fluid dynamics and further studies are needed for their applications, for example, as spreading agents which are of importance in the areas of nano- and microfluidics, surface coating, adhesion, and so on.

The dynamic nature of this phenomenon also allowed us to tune the structural shapes by changing other time-dependent parameters like the evaporation rate. In particular, we performed drop-casting experiments under a saturated solvent atmosphere (see the Supporting Information). In the above experiments the rate at which the liquid−vapor interface approaches the substrate is predominant with respect to the diffusion rate of POMs within the drop, however when the evaporation rate is slowed down, the assembly dynamics is expected to be governed by diffusion.[52] Thus, we found the formation of different structures by slowing down the evaporation time up to several minutes, exploiting an acetonitrile saturated environment. These include dendritic structures which are just typically observed in diffusion limited processes[53] (see Figure S5 of the Supporting Information showing characteristic features obtained for compounds **1**−**3**).

2.2.1. Tuning the Supramolecular Architectures of Different POMs by High Wetting Conditions. POMs with different chemical structures like clusters **1**, **2**, and **3** show different supramolecular architectures on SiOH under high wetting conditions. By comparing the peanut-like shape of cluster **1** the atypical shrink-wrapped cluster **2** and the planar discoid shape of **3**, we focus on the role that the structural features of these clusters may play on their surface assembly behavior. Such an interest arises due to the fact that different Dawson types show a very similar peanut-like shape but have different compositions, yet revealed the same morphology when drop-cast on SiOH (see compounds **8**−**13** in Figures S1 and S6 of the Supporting Information).

As shown in Figure 5, cluster **1** on SiOH reveals a porous 3D network consisting of 20−200 nm wide and about 1 nm deep holes (see section analysis in Figure 5b) and SFM scratching showed an average film thickness of about 4 nm (Figure S7 in the Supporting Information). By considering the cluster dimensions and the above data, Figure 5c shows how POM molecules could be arranged into a 3D layer-by-layer configuration where a single layer is imagined to be composed by interconnected POM molecules having their molecular main axis almost parallel to the surface plane.

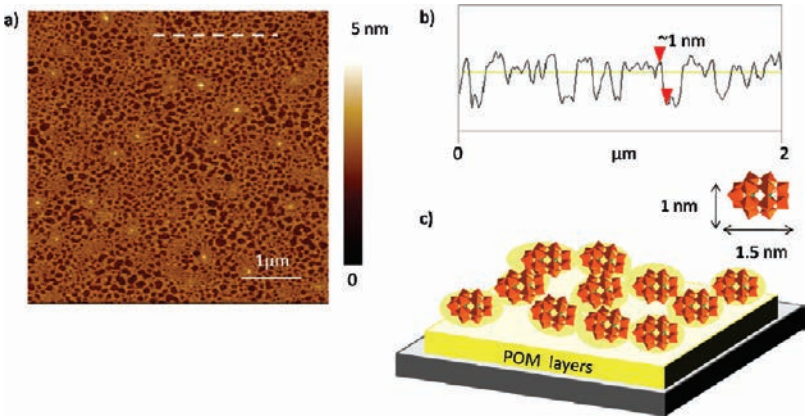

Figure 5. Compound **1** drop-cast on SiOH: (a) SFM image; (b) section analysis along the dashed line marked in part a; (c) picture sketching the intermolecular lateral interaction in the ultimate layer of the POM layer-by-layer deposit.

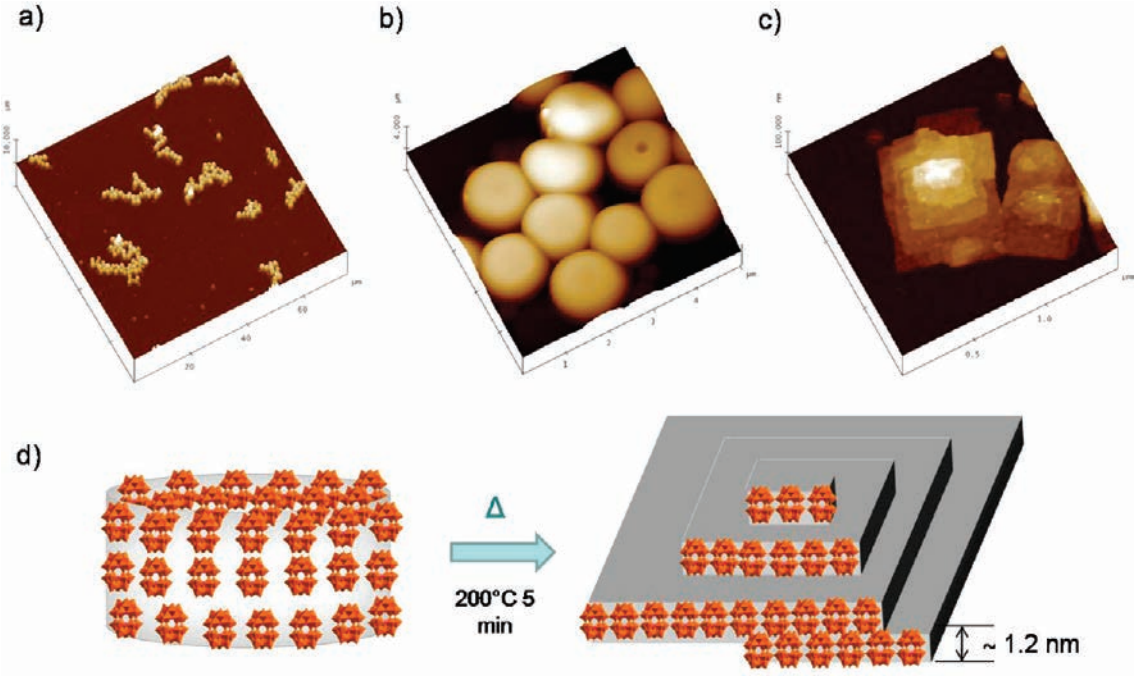

Figure 6. Compound **2** clusters drop-cast on a SiOH-rich surface: (a) SFM image of the grape-like arrangements; (b) zoom in a restricted representative region of part a; (c) SFM image of representative layered screw structures obtained upon thermal treatment; (d) pictorial sketch showing the morphological transition by a fully compact pancake-like structure to a layered screw, obtained by thermal treatment.

The plausibility of such a scenario is aided by considering the possible H-bonding interactions between the clusters, leading toward chain structures as shown in the solid state by single crystal X-ray data of this compound.[37] Accordingly, the TBA cations, which can undergo C−H···O H-bonded interactions with the cluster oxygen ligands,[54] are expected to be occupying the space between the adjacent cluster units. However, a further important factor for the observed assembling behavior can be ascribed to the strong POM−surface interaction arising due to the hydrophilic character of both systems, i.e., the arrangement in which the cluster axis parallel to the surface maximizes the cluster/surface contact.

The surface assembly formed by cluster **2** (see Figure 6) on SiOH shows a grape-like arrangement of pancake-like POM structures (Figure 6a). The zoom-in (Figure 6b) shows the details of these large structures, with the average dimensions of 700 nm tall and 1500 nm wide, which in some cases seem to be slightly deformed due to the pressure from the neighboring architectures. Moreover, the presence of these peculiar structures points to a remarkably low affinity between the Dawson-like cluster **2** on SiOH, and a similar effect has been observed for rigid-rod conjugated organic−inorganic hybrid POM nanodumbbells.[55] Here, the authors proposed a rough self-assembly process, whereby the anions and cations present in these compounds exist as single ions in polar solvent and attract each other via electrostatic interactions during the volatilization of the solvent. Such an interpretation was supported by the fact that these aggregates were not formed in solution and that their aggregation occurred on different substrates (silicon, HOPG, carbon-coated copper TEM grid), showing a poor influence of surfaces on their self-assembly.

This seems not to be the case for our systems, as remarkable surface effects are observed depending on both solution concentration (see Figure S8 of the Supporting Information) and surface hydrophilicity (see above describing different behavior on $SiCH_3$).

Moreover, differently from the various vesicle structures reported starting from POM building units,[54,56] whose formation is in some cases guided by surfactant cations in solution,[57,58] the structures observed in Figure 6 a,b are found to be fully compact, as indicated by SFM scratching experiments. Thus, the removal of hundreds of layers by pushing the SFM tip against individual pancake structures results in the visualization of massive structures (Figure S9 in the Supporting Information), thereby consisting of close-packed molecules more likely arranged as schematized in Figure 6d. Also, thermal treatment (200 °C for 5 min) of these systems led to the formation of layered screw dislocations and/or defined planes of crystallization which corresponds to the thermal oxidation of the encapsulated sulfite ions[59] as well as to an energy minimization effect of the self-assembled structures. Indeed, crystallization onto surfaces is generally referred to the formation of solid crystals by reorganization of previously deposited thin films. Nano- and microcrystals can develop in different shapes and dimensions, and this pancake-to-plane transition appears to be an unprecedented example. The same thermal treatments do not give rise to any significant modification of the assembled structures for the other compounds studied here.

Note that compound **2** differs from the others also for the counterion (tetrapentylammonium instead of TBA). Interestingly, by coupling compound **2** with TBA (namely, compound **14**), the same pancake-like structures, which crystallize in squared screws after thermal annealing, are observed (see Figure S10 in the Supporting Information). Thus, in this case, we may conclude that the anion plays a major role in the surface assembly phenomenon.

The morphology formed by the surface assembly of cluster **3** on SiOH is shown in Figure 7 where the tendency to form spiral-like architectures within micrometric grains is observed (in Figure 7a and in its magnification of Figure 7b). The spirals (see the dashed line in Figure 7b) consist of wrapped and flexible planes with a typical monomolecular interplanar distance of 0.8−1.2 nm which is consistent with the diameter of **3**. Moreover, the presence of dislocation defects is highlighted by the arrows in Figure 7b. This observation is interesting, since the formation of monomolecular planes is unique to cluster **3**, the only discoid-cage shaped cluster. Moreover, a close look at the chemical structure of this system suggests that the disk-to-disk interaction might be strengthened by hydrogen bonds between the organic pendants and adjacent clusters via C—H···O═Mo interactions.

2.2.2. Improved Lamellar Rigidity from Clusters with Organic Tails. The interesting lamellar assembly of cluster **3** led us to investigate strategies to modulate the planar rigidity. In particular, we inspect the effect of the derivatization of POM clusters by both organic tails and aromatics moieties and here the surface assembly behavior of compounds **4**−**7** on SiOH under high wetting conditions is reported.

Parts a and b of Figure 8 show, respectively, the height images of compounds **4** and **5** on SiOH, these systems being characterized by the Mn-Anderson core structure of cluster **3** functionalized by alkyl moieties of different length (see Figure 1). By analyzing in detail the images of clusters **3**, **4**, and **5** (see Figures 7b, 8a, and 8b), one can observe that the presence of the alkyl tails with increasing length produce a closer grain connection along with a few topological effects. Since we performed a comparative statistical analysis of the grain size distribution of these different systems, we found that no important variation in the mean grain size and standard deviation ~1.3 ± 0.55 μm have been observed for compounds **3** and **4**, thus suggesting that the addition of the two short tails (9 carbon

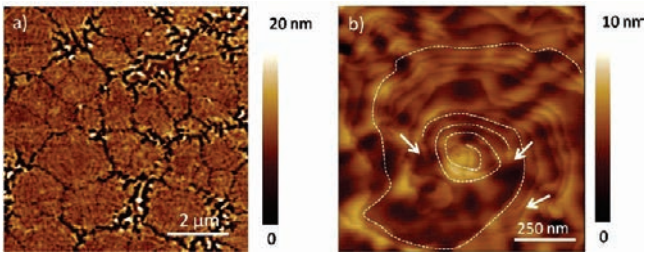

Figure 7. Cluster **3** drop-cast on a SiOH surface: (a) SFM large scale image; (b) zoom in a restricted region of part a.

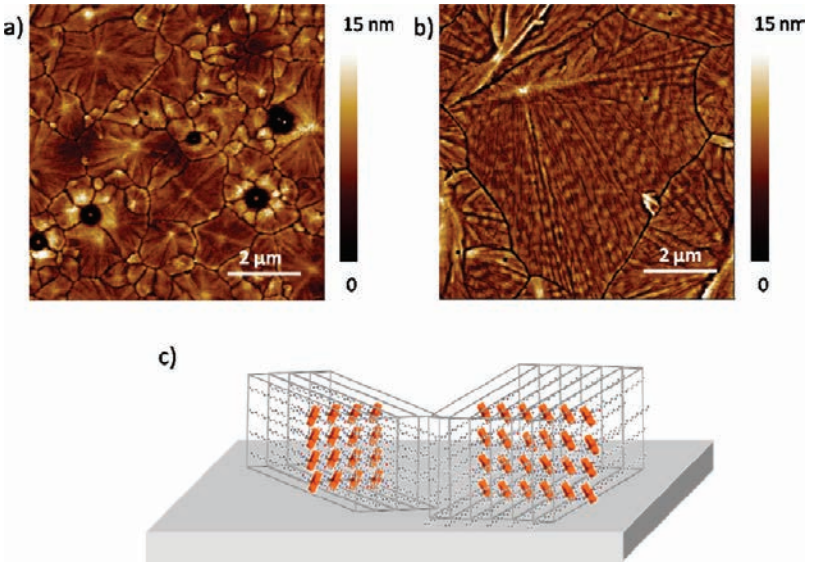

Figure 8. SFM images of clusters **4** (a) and **5** (b) drop-cast on SiOH. (c) Scheme showing the possible aggregation in lamellas with monomolecular size.

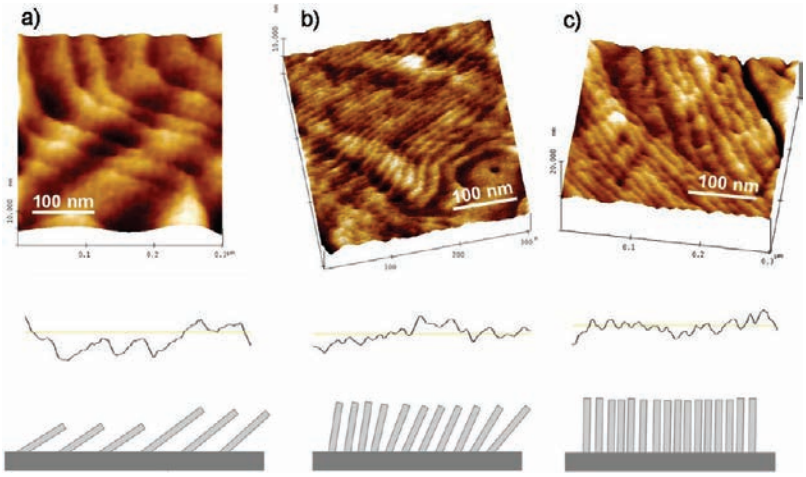

Figure 9. Topographic details (top) and schemes of monolayer stacking at the substrate surface (bottom) of (a) the inner part of a spiral-like grain of cluster **3** and (b, c) the inner part of lamellar grains of clusters **4** and **5**, respectively. Note that section analyses are reported on different *x*, *z* scales.

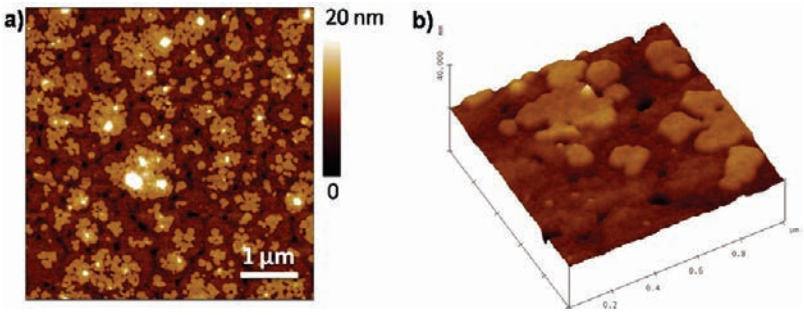

Figure 10. SFM images of compound **6** onto SiOH: (a) large scale image; (b) 3D images in a restricted region of part a.

atoms each) does not play an important role in modulating the grain size. On the other hand, compound **5** (18 carbon atoms backbone for each alkyl tail) presents a mean grain size value of 3.9 μm and a standard deviation of 1.8 μm, indicating that the growth process may be importantly affected by the employment of longer tails leading to larger grains. In contrast to cluster **3**, grain fracturing processes are observed for **4** and **5** whereby fracturing might be ascribed to the larger rigidity induced by the presence of the alkyl tails. Nevertheless, the monomolecular-plane structure of cluster **3** is evidenced in both **4** and **5** (see the detail of Figure 9). However, compounds **4** and **5** result in a higher structural rigidity than cluster **3** as their growth mode changes from spiral-like to lamellar. Further, in Figure 9, the organization of monomolecular planes inside the grains of cluster **3** (9a), **4** (9b), and **5** (9c) is compared. The monomolecular planes of cluster **3** reveal some flexibility (tendency to tilt and wrap up) that gradually disappears for clusters **4** and **5**, where the aforementioned planes are mostly perpendicular to the substrate and stack each other within long lamellar systems, and this allows us to conclude that, by adding alkyl tails to cluster **3**, plane rigidity along with lamellar systems are obtained.

Straight lamellar assembly and nanostructures formed by rolling of planes has been reported[60−62] for Keggin-type POM clusters, whereas dimethyldioctadecylammonium has been used as the countercation. Due to the long chain cations acting as organic surfactants, in these systems, the countercation has been shown to play a fundamental role in defining the assembly bulk features. In our case, we showed that similar arrangements may be obtained for ultrathin films on surfaces by properly functionalizing the POM cluster core.

2.2.3. The Surface Assembly of Multifunctional POM Derivatives. Figure 10 shows the SFM topography of compound **6** on SiOH, showing the different architecture obtained by an asymmetrically derived Mn-Anderson cluster with one alkyl tail and one pyrene unit (see Figure 1). The interest in this type of structure derives from the potentiality for it to act as a multifunctional hybrid POM, in which the alkyl tail would give a structural function and the POM cluster with the aromatic moiety could introduce other properties (optical, electrical, chemical). The film exhibits a dendritic LbL growth, and the reported SFM images show a lower, almost compact crystalline layer (large grains of 400−900 nm) and an upper submonolayer (small grains about 2 nm tall and 100−300 nm wide).

The height of the upper grains is consistent with a scenario where the molecules are tilted with respect to the substrate surface plane. In contrast, it is noteworthy to recall that the layered structure with 4 nm step height has also been found for the same compound on $SiCH_3$ (Figure 3), a picture in which the molecular systems tend to lay perpendicular with respect to that with the surface as an effect of the strong intermolecular interactions. Compound **7** (Figure 11) allowed us to observe this assembly effect induced by derivatizing the POM clusters with one more pyrene moiety. In contrast to compound **6**, compound **7** shows smaller (300−400 nm wide) and taller (about 4 nm) grains, indicating a perpendicular molecular orientation with respect to the surface plane.

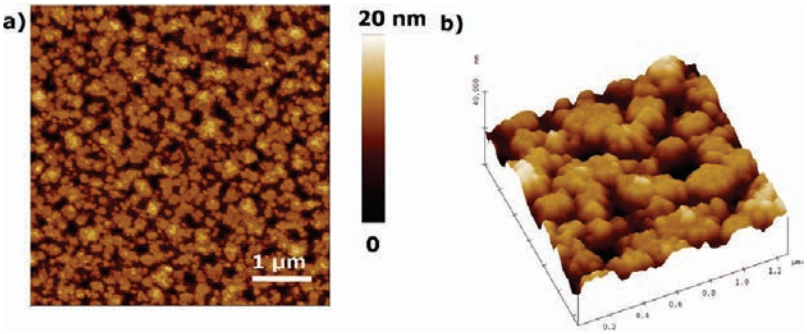

Figure 11. SFM images of compound **7** deposited onto SiOH: (a) large scale image; (b) 3D images in a restricted region of part a.

The comparison of the morphology of **6** and **7** is consistent with a picture in which surface assembly of hybrid POMs might be strongly influenced by the $\pi-\pi$ intermolecular stacking of small aromatic moieties.

CONCLUSIONS

When a POM-based nanostructure comes into contact with a solid surface via solution deposition, a wide landscape of assembled architectures is expected and the formation of 0D (dots, pancakes), 2D (lamellas), or 3D (porous networks, screws, plane-by-plane buildings) architectures may be tuned by both physical and chemical means. Additionally, our studies show the peculiarity of POMs to finely tune the spreading of fluids on hydrophilic surfaces and their dynamics, but further studies are necessary to quantify and explore the possibility to utilize the POMs for application as spreading agents, especially to deconvolute the contributions of the cations. Also, the derivatization of POM backbones by organic molecules is a very important tool, along with the supramolecular features, to tune the observed properties like structural rigidity and molecular orientation. Finally, the ordered LbL growth of POM hybrids derivatized by aromatic moieties on both hydrophobic and hydrophilic silicon-based substrates opens important perspectives for the exploitation of multifunctional POMs in many important technological fields including microelectronics, sensors, and photovoltaics.

EXPERIMENTAL SECTION

Polyoxometalates. The synthesis and structural characterization of the polyoxometalates studied here, viz., $TBA_6[H_2V\text{-}Mo_{17}O_{54}(VO_4)_2]$ (**1**),[37] $(C_{20}H_{44}N)_4[Mo_{18}O_{60}S_2]$ (**2**),[34,35] $TBA_3[MnMo_6O_{18}\{(OCH_2)_3C-NH_2\}_2]$ (**3**),[38] $TBA_3[MnMo_6O_{18}\{(OCH_2)_3C-C_9H_{17}\}_2]$ (**4**),[39] $TBA_3[MnMo_6O_{18}\{(OCH_2)_3C-NHCO-C_{17}H_{35}\}_2]\cdot 2C_3H_7NO$ (**5**),[36] $TBA_3[MnMo_6O_{18}((OCH_2)_3C-C_9H_{17})((OCH_2)_3CNH-CH_2-C_{16}H_9)]$ (**6**),[39] and $TBA_3[MnMo_6O_{18}\{(OCH_2)_3CNH-CH_2-C_{16}H_9\}_2]$ (**7**),[40] are reported elsewhere. In order to study the self-organization of these different POM systems on surfaces, 1 mg/mL concentrated solutions in acetonitrile (99.9%, Sigma Aldrich) (compounds **1**−**3** and **5**−**7**), or in a 1:1 mixture of acetonitrile and chloroform (99.9%, Sigma Aldrich) (compound **4**), were prepared and deposited via drop-casting on surfaces with different chemistries and wettabilities.

Substrate Surface Preparation and Characterization. Monocrystalline silicon wafers were used as substrates, and two different treatments were employed in order to obtain both highly hydrophilic (SiOH rich) and hydrophobic ($SiCH_3$ rich) surfaces.

SiOH rich surfaces were obtained by oxygen plasma treatment (March Instrument Plasmod-type Barrel) at a pressure of 1 mbar and a power of 75 W for 10 min, to clean and enhance the −OH surface density along with the surface hydrophilicity. As previously reported,[63] XPS of these surfaces showed only Si and O signals with no carbon contamination. In particular, the atomic percentage of oxygen measured from the O 1s component at about 532.8 eV was about a factor of 4 larger than that of silicon measured from the Si 2p component at about 103.7 eV. A water contact angle of about 10° was measured on these samples. These substrates were quite flat with a root-mean-square roughness (rms) of about 0.2 nm as measured on 1 μm^2 SFM images.

$SiCH_3$ surfaces were obtained by the above oxygen plasma treatment followed by surface functionalization with 1,1,1,3,3,3-hexamethyldisilazane (HMDS) (Sigma-Aldrich, semiconductor grade). As previously reported,[63] XPS on these surfaces showed Si, O, and C signals. In particular, the presence of a Si component at 101.8 eV indicates the formation of $Si-CH_3$ moieties. This is confirmed by the fact that the above component stays in a ratio of about 1/3 with respect to the total carbon content. An average water contact angle of 80° was measured on these samples. The roughness of $SiCH_3$ was about 0.3 nm on 1 μm^2 SFM images.

X-ray photoelectron spectroscopy (XPS) was carried out by using a Kratos AXIS-HS spectrometer. The Mg Kα1,2 of 1253.6 eV was used at the conditions of 10 mA and 15 keV with a pass energy of 40 eV. During the analysis, the residual pressure in the chamber was of the order of 10^{-7} Pa. The binding energy scale was referred to the lowest BE C 1s component at 284.8 eV. Spectra fitting have been done after linear background subtraction by using VISION Software (Version 1.4.0) by Kratos Analytical. Quantitative data were obtained by using experimentally derived atomic sensitivity factors.

Contact angle measurements were performed by a Kernco instrument at room temperature by using 1 μL drops of pure deionized water (ρ = 17 MΩ cm).

Scanning Force Microscopy. Dynamic scanning force microscopy (SFM) was carried out in air using a commercial instrument (MultimodeNanoscope IIIa, Digital Instruments, Santa Barbara, California) equipped with a phase extender apparatus and a Q-box module.[64,65] Etched-silicon probes with a pyramidal-shape tip having a nominal curvature of 10 nm and a nominal internal angle of 35° were used. During the scanning, the 125-μm-long cantilever, with a nominal spring constant in the range 20−100 N m, oscillated at its resonance frequency (∼330 kHz). Height and phase images were collected by capturing 512 × 512 points in each scan, and the scan rate was maintained

below 1 lines per second. During the imaging, temperature and humidity were about 293 K and 40%, respectively. The thicknesses of the POM layers were measured by employing the SFM scratching method. Accordingly, the SFM tip was pushed against the surfaces with a high load and a $1 \times 1\ \mu m^2$ size scan was performed on the surface. This allowed for the removal of POM layers, leading to square holes. The depths of the square holes were measured by section analysis.

■ ASSOCIATED CONTENT

Supporting Information. Representation of compounds **8**−**13**; structural homogeneity of drop-cast film on SiOH substrates; dewetting-induced mounds of compounds **2**−**13**; self-organization of compounds **1**−**3** under a solvent saturated environment; 3D porous networks formed by drop-casting compounds **8**−**13**; AFM scratched area of a thin film of cluster **1** on SiOH; concentration effect for compound **2** drop-cast on SiOH; scratching experiments on cluster **2** supramolecular structures onto SiOH; surface organization of compound **14** on SiOH. This material is available free of charge via the Internet at http://pubs.acs.org.

■ AUTHOR INFORMATION

Corresponding Author

*E-mail: bruno.pignataro@unipa.it (B.P.); L.Cronin@chem.gla.ac.uk (L.C.).

■ ACKNOWLEDGMENT

The authors acknowledge Italian MiUR (PRIN 2008, FIRB-Futuro in Ricerca), the University of Palermo, the EPSRC, and WestCHEM for financial support, L.C. thanks the Royal Society/Wolfson Foundation for the award of a merit award, and H.N.M. thanks the Royal Society of Edinburgh.

■ REFERENCES

(1) Long, D. L.; Burkholder, E.; Cronin, L. *Chem. Soc. Rev.* **2007**, 36.
(2) Pope, M. T.; Müller, A. *Angew. Chem., Int. Ed. Engl.* **1991**, *30*, 34.
(3) Kögerler, P.; Cronin, L. *Angew. Chem., Int. Ed.* **2005**, *44*, 844.
(4) Yamase, T. *Chem. Rev.* **1998**, *98*, 307.
(5) Rhule, J. T.; Neiwert, W. A.; Hardcastle, K. I.; Do, B. T.; Hill, C. L. *J. Am. Chem. Soc.* **2001**, *123*, 12101.
(6) Vasylyev, M. V.; Neumann, R. *J. Am. Chem. Soc.* **2004**, *126*, 884.
(7) Mizuno, N.; Yamaguchi, K.; Kamata, K. *Coord. Chem. Rev.* **2005**, *249*, 1944.
(8) Mizuno, N.; Misono, M. *Chem. Rev.* **1998**, *98*, 199.
(9) Sadakane, M.; Steckhan, E. *Chem. Rev.* **1998**, *98*, 219.
(10) Müller, A.; Kögerler, P.; Dress, A. W. M. *Coord. Chem. Rev.* **2001**, *222*, 193.
(11) Yamase, T.; Fukaya, K.; Nojiri, H.; Ohshima, Y. *Inorg. Chem.* **2006**, *45*, 7698.
(12) Clemente-Juan, J. M.; Coronado, E. *Coord. Chem. Rev.* **1999**, *193*−*195*, 361.
(13) Long, D. L.; Kogerler, P.; Farrugia, L. J.; Cronin, L. *Dalton Trans.* **2005**, 1372.
(14) Klemperer, W. G.; Wall, C. G. *Chem. Rev.* **1998**, *98*, 297.
(15) Fleming, C.; Long, D.-L.; McMillan, N.; Johnson, J.; Bovet, N.; Dhanak, V.; Gadegaard, N.; Kögerler, P.; Cronin, L.; Kadodwala, M. *Nat. Nanotechnol.* **2008**, *3*, 229.
(16) Ge, M.; Zhong, B.; Klemperer, W. G.; Gewirth, A. A. *J. Am. Chem. Soc.* **1996**, *118*, 5812.
(17) Ge, M.; Niece, B. K.; Wall, C. G.; Klemperer, W. G.; Gewirth, A. A. *Mater. Res. Soc. Symp. Proc.* **1997**, *451*, 99.
(18) Keïta, B.; Nadjo, L. *Surf. Sci. Lett.* **1991**, *254*, L443.
(19) Song, I. K.; Kaba, M. S.; Coulston, G.; Kourtakis, K.; Barteau, M. A. *Chem. Mater.* **1996**, *8*, 2352.
(20) Kurth, D. G.; Volkmer, D. In *Polyoxometalate Chemistry: From Topology via Self-Assembly to Applications*; Pope, M. T., Müller, A., Eds.; Kluwer Academic: Dordrecht, 2001; p 301.
(21) Decher, G. *Science* **1997**, *277*, 1932.
(22) Liu, S.; Volkmer, D.; Kurth, D. G. *J. Cluster Sci.* **2003**, *14*, 405.
(23) Clemente-León, M.; Mingotaud, C.; Agricole, B.; Gómez-García, C. J.; Coronado, E.; Delhaes, P. *Angew. Chem., Int. Ed.* **1997**, *36*, 1114.
(24) Volkmer, D.; Chesne, A. D.; Kurth, D. G.; Schnablegger, H.; Lehmann, P.; Koop, M. J.; Müller, A. *J. Am. Chem. Soc.* **2000**, *122*, 1995.
(25) Clemente-Leon, M.; Coronado, E.; Gomez-Garcia, C. J.; Mingotaud, C.; Ravaine, S.; Romualdo-Torres, G.; Delhaes, P. *Chem.—Eur. J.* **2005**, *11*, 3979.
(26) Errington, R. J.; Petkar, S. S.; Harrocks, B. R.; Houlton, A.; Lie, L. H.; Patole, S. N. *Angew. Chem., Int. Ed.* **2005**, *44*, 1254.
(27) Bu, W.; Li, H.; Sun, H.; Yin, S.; Wu, L. *J. Am. Chem. Soc.* **2005**, *127*, 8016.
(28) Pradeep, C. P.; Long, D.-L.; Newton, G. N.; Song, Y.-F.; Cronin, L. *Angew. Chem., Int. Ed.* **2008**, *47*, 4388.
(29) Proust, A.; Thouvenot, R.; Gouzerh., P *Chem. Commun.* **2008**, 1837.
(30) Song, Y.-F.; McMillan, N.; Long, D.-L.; Kane, S.; Malm, J.; Riehle, M. O.; Pradeep, C. P.; Gadegaard, N.; Cronin, L. *J. Am. Chem. Soc.* **2009**, *131*, 1340.
(31) Raudino, A.; Pignataro, B. *J. Phys. Chem. B* **2007**, *111*, 9189.
(32) Pignataro, B. *J. Mater. Chem.* **2009**, *19*, 3338.
(33) Fabiano, S.; Pignataro, B. *Phys. Chem. Chem. Phys.* **2010**, *12*, 14848.
(34) Baffert, C.; Boas, J. F.; Bond, A. M.; Kögerler, P.; Long, D.-L.; Pilbrow, J. R.; Cronin, L. *Chem.—Eur. J.* **2006**, *12*, 8472.
(35) Long, D.-L.; Kögerler, P.; Cronin, L. *Angew. Chem., Int. Ed.* **2004**, *43*, 1817.
(36) Song, Y.-F.; McMillan, N.; Long, D.-L.; Thiel, J.; Ding, Y.; Chen, H.; Gadegaard, N.; Cronin, L. *Chem.—Eur. J.* **2008**, *14*, 2349.
(37) Miras, H. N.; Long, D.-L.; Kögerler, P.; Cronin, L. *Dalton Trans.* **2008**, 214.
(38) Marcoux, P. R.; Hasenknopf, B.; Vaissermann, J.; Gouzerh, P. *Eur. J. Inorg. Chem.* **2003**, 2406–2412.
(39) Rosnes, M. H.; Musumeci, C.; Pradeep, C. P.; Mathieson, J. S.; Long, D.-L.; Song, Y.-f.; Pignataro, B.; Cogdell, R.; Cronin, L. *J. Am. Chem. Soc.* **2010**, *132*, 15490.
(40) Song, Y.-F.; Long, D.-L.; Cronin, L. *Angew. Chem., Int. Ed.* **2007**, *46*, 3900.
(41) Long, D.-L.; Kogerler, P.; Farrugia, L. J.; Cronin, L. *Angew. Chem., Int. Ed.* **2003**, *42*, 4179.
(42) McHale, G.; Rowan, S. M.; Newton, M. I.; Banerjee, M. K. *J. Phys. Chem. B* **1998**, *102*, 1964.
(43) Zhong, D. Y.; Hirtz, M.; Wang, W. C.; Dou, R. F.; Chi, L. F.; Fuchs, H. *Phys. Rev. B* **2008**, *77*, 113404.
(44) Okumura, H.; Horita, M.; Kimoto, T.; Suda, J. *Appl. Surf. Sci.* **2008**, *254*, 7858.
(45) Tonchev, V.; Ranguelov, B.; Omi, H.; Pimpinelli, A. *Eur. Phys. J. B* **2010**, *73*, 539.
(46) Deegan, R. D. *Phys. Rev. E* **2000**, *61*, 475.
(47) Deegan, R. D.; Bakajin, O.; Dupont, T. F.; Huber, G.; Nagel, S. R.; Witten, T. A. *Nature* **1997**, *389*, 827.
(48) Wasan, D. T.; Nikolov, A. D. *Nature* **2003**, *423*, 156.
(49) Thiele, U.; Mertig, M.; Pompe, W. *Phys. Rev. Lett.* **1998**, *80*, 2869.
(50) Chengara, A.; Nikolov, A. D.; Wasan, D. T.; Trokhymchuk, A.; Henderson, D. *J. Colloid Interface Sci.* **2004**, *280*, 192.
(51) Craster, R. V.; Matar, O. K.; Sefiane, K. *Langmuir* **2009**, *25*, 3601.

(52) Bigioni, T. P.; Lin, X.-M.; Nguyen, T. T.; Corwin, E. I.; Witten, T. A.; Jaeger, H. M. *Nat. Mater.* **2006**, *5*, 265.
(53) Witten, J., T. A.; Sander, L. M. *Phys. Rev. Lett.* **1981**, *47*, 1400.
(54) Pradeep, C. P.; Misdrahi, M. F.; Li, F.; Zhang, J.; Xu, L.; Long, D.-L.; Liu, T.; Cronin, L. *Angew. Chem., Int. Ed.* **2009**, *48*, 8309.
(55) Zhu, Y.; Wang, L.; Hao, J.; Xiao, Z.; Wei, Y.; Wang, Y. *Cryst. Growth Des.* **2009**, *9*, 3509.
(56) Zhang, J.; Song, Y.-F.; Cronin, L.; Liu, T. *J. Am. Chem. Soc.* **2008**, *130*, 14408.
(57) Fan, D.; Hao, J. *J. Colloid Interface Sci.* **2010**, *342*, 43.
(58) Yan, Y.; Wang, H.; Li, B.; Hou, G.; Yin, Z.; Wu, L.; Yam, V. W. W. *Angew. Chem., Int. Ed.* **2010**, *49*, 9233.
(59) Long, D.-L.; Kogerler, P.; Cronin, L. *Angew. Chem., Int. Ed.* **2004**, *43*, 1817.
(60) Nyman, M.; Rodriguez, M. A.; Anderson, T. M.; Ingersoll, D. *Cryst. Growth Des.* **2009**, *9*, 3590.
(61) Nisar, A.; Zhuang, J.; Wang, X. *Chem. Mater.* **2009**, *21*, 3745.
(62) Nisar, A.; Lu, Y.; Wang, X. *Chem. Mater.* **2010**, *22*, 3511.
(63) Musumeci, C.; Cascio, C.; Scandurra, A.; Indelli, G. F.; Bongiorno, C.; Ravesi, S.; Pignataro, B. *Surf. Sci.* **2008**, *602*, 993.
(64) Pignataro, B.; Chi, L. F.; Gao, S.; Anczykowski, B.; Niemeyer, C. M.; Adler, M.; Blohm, D.; Fuchs, H. *Appl. Phys. A: Mater. Sci. Process.* **2002**, *74*, 447.
(65) Pignataro, B.; Sardone, L.; Marletta, G. *Nanotechnology* **2003**, *14*, 245.